

Surface Modification with Metal Hexacyanoferrates for Expanding the Choice of H₂-Evolving Photocatalysts for Both Fe³⁺/Fe²⁺ Redox-Mediated and Interparticle Z-Scheme Water-Splitting Systems

Hikaru Matsuoka, Tomoki Inoue, Hajime Suzuki, Osamu Tomita, Shunsuke Nozawa, Akinobu Nakada, and Ryu Abe*

The construction of Z-scheme water splitting systems is an effective approach toward harvesting a wide portion of the solar light spectrum; however, the success has often depended on the property of photocatalyst surfaces. This drawback is typified by the limited choice of efficient H₂ evolution photocatalysts (HEPs) (e.g., Rh-doped SrTiO₃) for Z-scheme water splitting using Fe³⁺/Fe²⁺ redox couple. The majority of visible light-responsive materials shows low activity for H₂ production with Fe²⁺ electron donors despite having suitable band levels, probably due to the absence of an effective surface site for oxidizing Fe²⁺. The choice of HEPs for interparticle Z-scheme systems has also been limited. Herein, an effective strategy for overcoming these limitations is reported: activation of originally inactive materials via surface modification with metal hexacyanoferrate nanoparticles. Photocatalytic H₂ evolution over TaON in aqueous Fe²⁺ solution is drastically enhanced by comodification with indium hexacyanoferrate (InHCF) and Rh–Cr mixed oxide. InHCF promotes Fe²⁺ oxidation to Fe³⁺ utilizing the holes photogenerated in TaON via Fe^{III}/Fe^{II} redox cycles, enabling Z-scheme water splitting with the Fe³⁺/Fe²⁺ redox mediator coupled with an O₂ evolution photocatalyst under visible light. It is also disclosed that InHCF nanoparticles function as effective solid electron mediators for achieving interparticle Z-scheme water splitting.

1. Introduction

Water splitting using particulate photocatalysts has been extensively studied because of the significant potential of this technology for large-scale clean hydrogen (H₂) production.^[1–5] Although the utilization of a wide portion of the visible spectrum is indispensable for achieving practically sufficient solar-to-hydrogen (STH) conversion efficiencies, there are only a few examples of visible light-driven water-splitting systems using a single photocatalyst.^[6–12] This is primarily due to the strict requirements for the semiconductor materials, including a bandgap that is narrower than 3.1 eV, band levels suitable for both water reduction and oxidation, and high stability.


Z-scheme-type water splitting (Zs-WS) systems, which generally consist of two different particulate photocatalysts—one for H₂ evolution and the other for O₂ evolution—and a redox couple that dissolves in aqueous solutions, have been demonstrated to enable the use of various

visible light-responsive photocatalyst materials that do not meet the above criteria.^[13,14] However, the success of this strategy has often depended on the surface properties of photocatalysts such as affinity with redox couples, not only their band levels (i.e., thermodynamical requisites). Actually, many photocatalysts exhibit negligible H₂ or O₂ evolution in the presence of appropriate redox species, despite the suitability of their band levels for the target reactions with the redox species. Thus, the majority of previous Zs-WS systems using conventional redox couples (e.g., IO₃[−]/I[−] and Fe³⁺/Fe²⁺) have relied on the specific affinity such as the selective adsorption of either species onto the photocatalyst surface.^[2,15]

This problem is typified by the narrow selection of H₂ evolution photocatalysts (HEPs) applicable to Zs-WS using the Fe³⁺/Fe²⁺ redox couple.^[16–19] Due to several practical advantages of Fe³⁺/Fe²⁺, including an appropriate redox potential and a simple one-electron transfer process, it has been extensively studied.^[13,14] However, the highly efficient HEP with Fe²⁺ electron donor has so far been limited to Rh-doped SrTiO₃ (STO:Rh)

H. Matsuoka, T. Inoue, H. Suzuki, O. Tomita, A. Nakada, R. Abe
Department of Energy and Hydrocarbon Chemistry
Graduate School of Engineering
Kyoto University
Nishikyo-ku, Kyoto 615-8510, Japan
E-mail: ryu-abe@scl.kyoto-u.ac.jp

S. Nozawa
Photon Factory (PF)
Institute of Materials Structure Science (IMSS)
High Energy Accelerator Research Organization (KEK)
Tsukuba, Ibaraki 305-0801, Japan

 The ORCID identification number(s) for the author(s) of this article can be found under <https://doi.org/10.1002/solr.202300431>.

© 2023 The Authors. Solar RRL published by Wiley-VCH GmbH. This is an open access article under the terms of the Creative Commons Attribution-NonCommercial-NoDerivs License, which permits use and distribution in any medium, provided the original work is properly cited, the use is non-commercial and no modifications or adaptations are made.

DOI: 10.1002/solr.202300431

originally developed by Kudo and coworkers,^[19] along with some organic semiconductors showing moderate activity.^[17,18] In contrast, the availability of efficient O₂ evolution photocatalysts (OEPs) with Fe³⁺/Fe²⁺ redox is considerably greater (e.g., WO₃,^[16] BiVO₄,^[16] H₂WO₄,^[20,21] TiO₂:Ta,N,^[22] and Bi₄NbO₈Cl^[23]). Notably, undoped STO exhibited low H₂ evolution activity in the presence of an Fe²⁺ electron donor under UV light irradiation.^[16] This implies Rh species near surface presumably serve as specific sites for the oxidation of Fe²⁺.

Another class of Zs-WS systems is “interparticle” ones in which electron transfer between HEP and OEP takes place directly or via solid electron mediators even in the absence of redox couple dissolved in reaction solution. The first example was demonstrated using the combination of STO:Rh and BiVO₄ as HEP and OEP, respectively, without any solid electron mediators.^[24] Then various solid electron mediators such as reduced graphene oxide (RGO), Au, ITO nanoparticles, and carbon nanotube^[25–28] have been employed to facilitate electron transfer between HEP and OEP. About 1% of STH was recently achieved by Domen et al. using a photocatalyst panel consisting of STO:Rh (codoped with La and Rh), BiVO₄, and Au.^[26] Similar to the aforementioned Fe³⁺/Fe²⁺ redox case, most of interparticle Zs-WS systems still employ STO:Rh-based materials as highly efficient HEPs, while some others showing moderate activity such as metal sulfides have recently been developed.^[29] It has been suggested that the Rh cation species presumably serve as specific sites for the interparticle electron transfer, not only providing visible light absorption.^[24,30] Thus, to widen the choice of HEPs applicable in redox-mediated and/or interparticle Zs-WS systems, effective reaction sites that facilitate the oxidation of redox mediator and interparticle electron transfer, respectively, should be rationally designed on the photocatalyst surface.

Here, we focused on Prussian blue analogues, so-called metal hexacyanoferrates (MHCFs), as such facilitators. MHCFs are a class of 3D coordination polymers with a general formula of A_hM_k[Fe(CN)₆]_l·mH₂O (Figure 1; *h, k, l, m*: composition ratios; A: alkali metal cation; M: (transition) metal cation), where M and Fe ions are bridged by cyanide (CN) ligands.^[31] The MHCF family has attracted considerable attention as functional

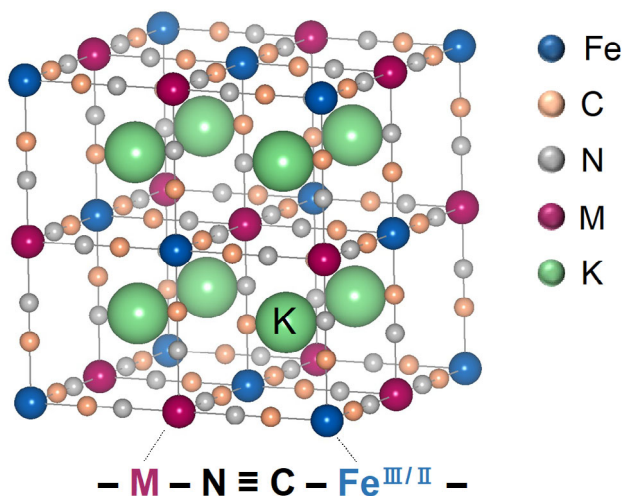


Figure 1. Typical structure of MHCF, K₂M[Fe(CN)₆].

materials applicable in various technologies, such as in electrochromic devices,^[32,33] adsorbents,^[34,35] electrodes for secondary batteries,^[36,37] and (electro)catalysis.^[38–40] Recently, we have demonstrated that the surface modification of metal sulfide or selenide photocatalysts (e.g., CdS) with MHCF (A = K⁺, M = Cd^{II}, Zn^{II}, or In^{II}) increases the H₂ evolution rate in the presence of [Fe(CN)₆]⁴⁻ as an electron donor. MHCF was found to promote [Fe(CN)₆]⁴⁻ oxidation via the reversible Fe^{III}/Fe^{II} redox cycles in MHCFs.^[41–43] These findings motivated us to employ MHCFs as facilitators for activating HEPs that have so far been inactive in the combination with specific redox mediators such as Fe³⁺/Fe²⁺.

2. Results and Discussion

2.1. Characterization of InHCF Nanoparticles

Indium hexacyanoferrate (InHCF) nanoparticles were prepared according to a previously published method for the preparation of MHCF nanoparticles containing either Fe, Co, or Ni cations,^[44] but not for In-contained one. Although no crystallographic data have been recorded in the ICDD for InHCF, the X-ray diffraction (XRD) patterns of the fabricated InHCF particles (Figure 2a) resembled those of previously reported InHCF samples with relatively large particle sizes (≈200 nm).^[45,46] The results of Le Bail refinement of the experimental XRD pattern (Figure S1, Supporting Information) supported the formation of InHCF sample composed of KIn[Fe(CN)₆] species. The no change in the XRD pattern of InHCF before and after heating at 373 K supports that the structure of InHCF should be maintained after loading on TaON (Figure 2a). The attenuated total reflectance–Fourier transform infrared spectroscopy (ATR–FTIR) spectra (Figure S2a, Supporting Information) of the InHCF samples contained absorption bands at ≈2100–2070 cm⁻¹, assignable to the stretching vibration mode of C≡N, as is generally observed in MHCFs,^[31] differing markedly from those of K₄[Fe(CN)₆]·3H₂O (2044 cm⁻¹) and its oxidized form K₃[Fe(CN)₆] (2117 cm⁻¹). The transmission electron microscopy (TEM) images of the InHCF samples (Figure 2b) revealed irregularly shaped nanoparticles with diameters < 100 nm.

The surface area was estimated to be 39.7 m² g⁻¹ using N₂ adsorption measurements and the Brunauer–Emmett–Teller (BET) method. The elemental composition of the InHCF sample, K_hIn_k[Fe(CN)₆]_l, was estimated using X-ray photoelectron spectroscopy (XPS) and inductively coupled plasma optical emission spectrometry (ICP–OES). The XPS analysis indicated that the ratio of K:In:Fe (*h:k:l*) was ≈0.7:1.0:0.9. The In:Fe ratio was close to that determined by ICP–OES (1.00:0.88). The difference from the ideal values (i.e., *h:k:l* = 1:1:1) may indicate the presence of defect sites, which has been suggested for Prussian blue and its derivatives.^[47,48] The MHCFs employed should exhibit good reversibility of the Fe^{III}/Fe^{II} redox cycle, with a redox potential appropriate for targeted photocatalysis. As shown in Figure 2c, reversible redox behavior with sharp peaks was observed in the cyclic voltammetry (CV) profiles of InHCF, and the half-wave potential (*E*_{1/2} = 0.93 V vs. standard hydrogen electrode (SHE), pH 2.5) of Fe^{III}/Fe^{II} agreed well with the literature values,^[49,50] which is

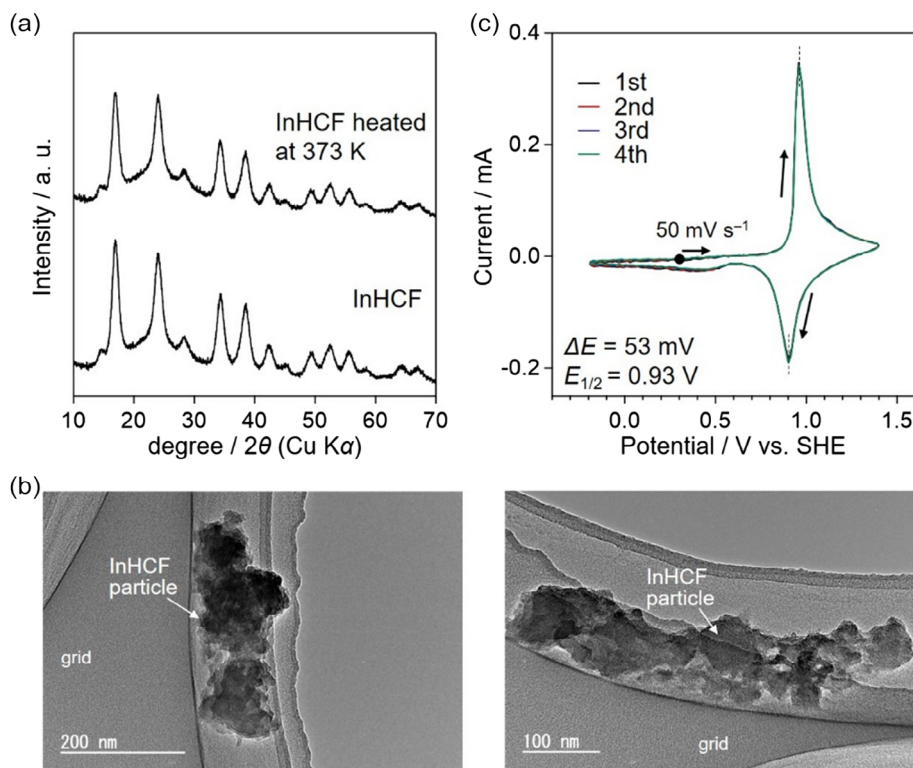
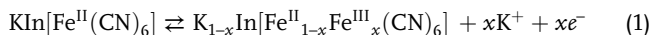


Figure 2. Characterization of InHCF nanoparticles: a) XRD patterns, b) TEM images, and c) cyclic voltammograms obtained using an InHCF nanoparticle-deposited FTO electrode at a scan rate of 50 mV s^{-1} in aqueous K_2SO_4 solution (0.1 M, 40 mL) at pH 2.5.

appropriate for the oxidation of Fe^{2+} cations in aqueous solution, being more positive than that of $\text{Fe}^{3+}/\text{Fe}^{2+}$ (0.77 V). As shown in Figure S3, Supporting Information, such good reversibility in $\text{Fe}^{\text{III}}/\text{Fe}^{\text{II}}$ redox was confirmed in the relatively wide range of pH from 2.5 to 6.0. Importantly, the $E_{1/2}$ values were almost independent on this pH range. The redox reaction occurring on InHCF can be thus described by Equation (1), where divalent and trivalent iron species coexist, as suggested in previous studies



where x is the number of moles of reacted electrons.

2.2. Characterization of TaON Modified with a Conventional H_2 Evolution Cocatalyst and InHCF

Figure S4, Supporting Information, shows the TEM images of TaON loaded with well-known H_2 evolution cocatalysts ($\text{Rh}_x\text{Cr}_{2-x}\text{O}_3$, Pt, or Rh), along with that of the unmodified sample. Hereafter, $\text{Rh}_x\text{Cr}_{2-x}\text{O}_3$ is denoted as RCO for simplification. Nanoparticles of RCO with an average diameter of 2 nm were highly dispersed on the surface of the TaON. In contrast, the Pt and Rh particle sizes were not homogeneous and were larger than those of RCO, with inferior dispersion. **Figure 3** shows TEM images of the RCO/TaON sample further modified with InHCF (InHCF/RCO/TaON), wherein it is evident that the TaON surface was densely covered by a layer of InHCF particles with a thickness of 20–100 nm. Although the relatively thick InHCF

layers obscured the preloaded RCO nanoparticles in the TEM images, characterization using XPS, XRD, and ATR-FTIR confirmed the presence of RCO species as well as the retention of their physicochemical properties (Figure S5 and S6, Supporting Information). Likewise, it was confirmed that the physicochemical properties of InHCF remained unchanged after loading onto TaON. Similar results were observed for the InHCF/Pt/TaON and InHCF/Rh/TaON samples (Figure S7–S10, Supporting Information).

2.3. Effects of InHCF Modification on H_2 Evolution in the Presence of Fe^{2+} Electron Donor

Figure 4 shows H_2 evolution using TaON photocatalysts and Fe^{2+} electron donor under visible light irradiation ($\lambda > 400 \text{ nm}$). Modification with either InHCF or RCO slightly enhanced the H_2 evolution activity; however, the resulting H_2 evolution rates were still exceedingly low ($< 5 \mu\text{mol h}^{-1}$). In contrast, the coloading of InHCF and RCO resulted in H_2 evolution at significantly higher rates ($104 \pm 14 \mu\text{mol h}^{-1}$). The optimized amounts of InHCF, Rh, and Cr were 10 mol%, 1, and 1.5 wt%, respectively (**Table 1**). The total amount of generated H_2 reached $659 \mu\text{mol}$, which is close to the stoichiometric amount ($625 \mu\text{mol}$) calculated based on the amount of added Fe^{2+} ($1250 \mu\text{mol}$), strongly suggesting that almost all Fe^{2+} cations were oxidized to Fe^{3+} by the photogenerated holes on TaON, accompanied by stoichiometric (i.e., two-electron) reduction of water to H_2 . The excess formation of H_2 can be rationalized by considering

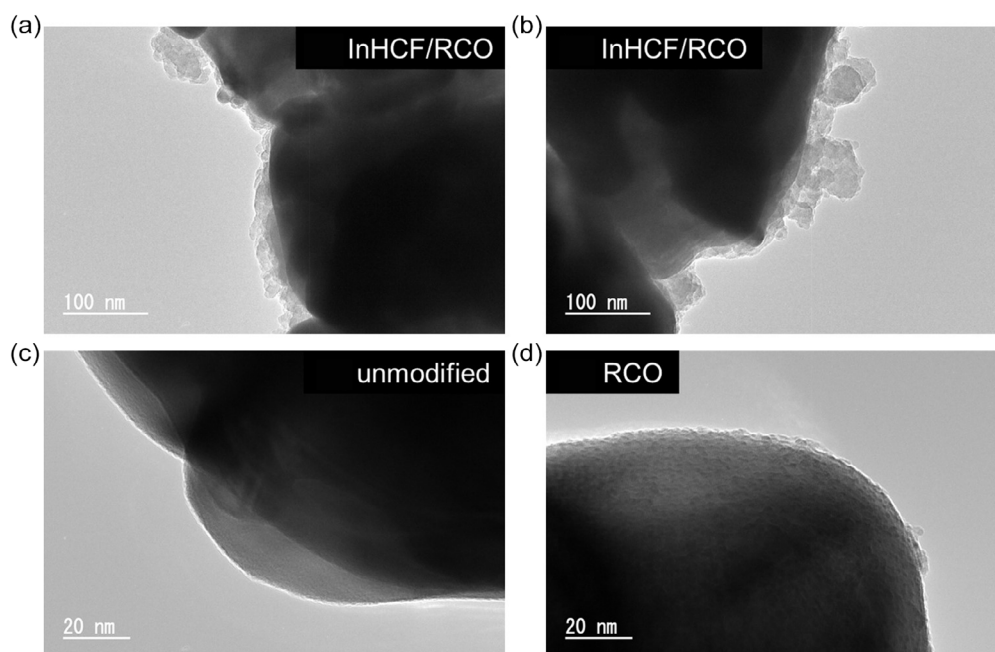


Figure 3. TEM images of a,b) InHCF/RCO/TaON, c) unmodified TaON, and d) RCO/TaON.

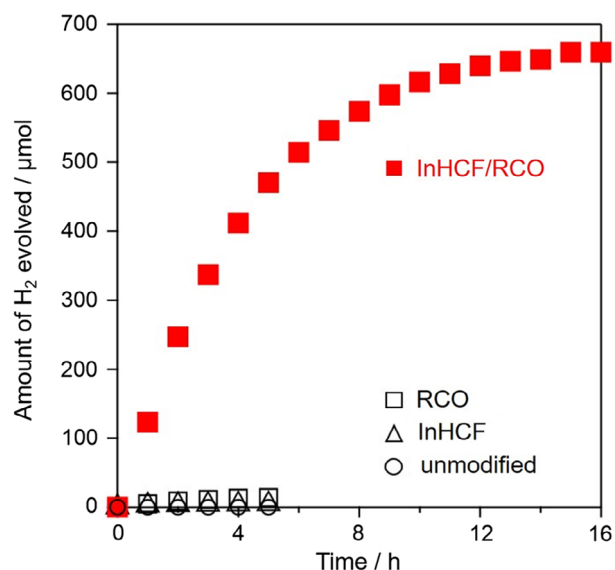


Figure 4. H₂ evolution with time over InHCF/RCO/, RCO/, or InHCF/TaON and unmodified TaON in aqueous FeCl₂ solution (5 mM, 250 mL) at pH 2.5 under visible light irradiation ($\lambda > 400$ nm).

the oxidation of residual organic contaminants and/or InHCF by holes, given that a small amount of H₂ (14 μ mol) was generated from InHCF/RCO/TaON in the absence of Fe²⁺ (Figure S11, Supporting Information). Neither modification with InCl₃ nor the simple addition of InHCF nanoparticles to the solution improved the activity of RCO/TaON (Figure S12, Supporting Information), indicating that the loading of InHCF species onto the TaON surface is essential for enhancing H₂ evolution. Importantly, no changes were observed in the XPS and

Table 1. Initial rates of H₂ evolution over TaON modified with various amounts of RCO and InHCF under visible light irradiation.

Rh added [wt%]	Cr added [wt%]	InHCF ^{a)} [mol%]	Activity [μ mol h ⁻¹]
0.50	0.75	10	51.9
1.00	1.50	10	104 \pm 14
1.50	2.25	10	84.0
1.00	0.50	10	77.8
1.00	3.00	10	93.2
1.00	1.50	5	63.9
1.00	1.50	15	103

^{a)}Loaded amount of InHCF was determined based on Fe content in InHCF which was regarded as KIn[Fe(CN)₆].

ATR-FTIR spectra of InHCF/RCO/TaON after the reaction (Figure S13, Supporting Information). The apparent H₂ evolution quantum efficiency of InHCF/RCO/TaON under similar conditions, but with monochromatic light, was 1.2% at 420 nm. **Figure 5** shows a comparison of the H₂ evolution activities of InHCF-modified and unmodified TaON preloaded with Pt or Rh instead of RCO. In both cases, coloading of InHCF promoted H₂ evolution, but the rates were substantially lower than those of InHCF/RCO/TaON.

2.4. Mechanism of H₂ Evolution Enhancement Due to Comodification of TaON with InHCF and RCO

The above results indicate that the InHCF species endows the originally inactive TaON photocatalyst with H₂ evolution activity

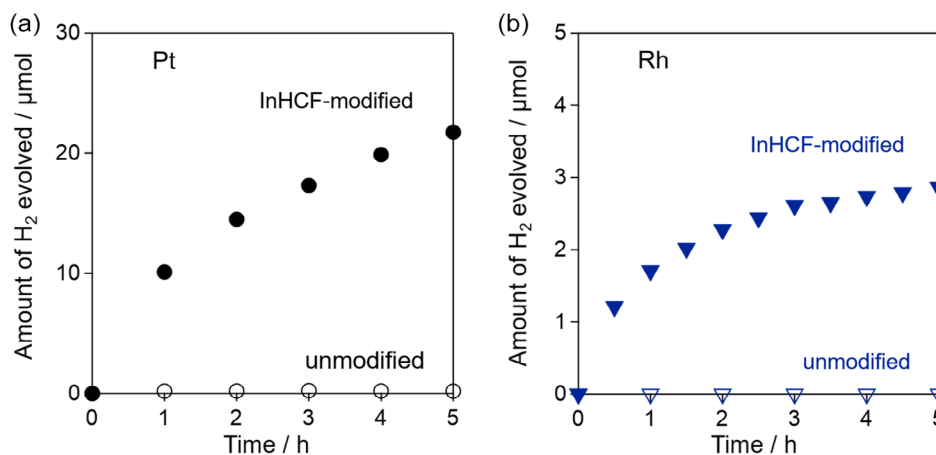


Figure 5. H₂ evolution with time over InHCF-modified or unmodified a) Pt/TaON or b) Rh/TaON in aqueous FeCl₂ solution (5 mM, 250 mL) at pH 2.5 under visible light irradiation.

using an Fe²⁺ electron donor. Presumably, the InHCF species function as specific Fe²⁺ oxidation sites, similar to the Rh cation species doped in SrTiO₃ semiconductor particles.^[30] This assumption is strongly supported by the finding that comodification with InHCF promoted H₂ evolution from aqueous Fe²⁺, regardless of the type of reduction cocatalysts (RCO, Pt, or Rh), to a greater or lesser extent (Figure 4 and 5). Notably, TaON loaded solely with InHCF did not exhibit H₂ evolution when methanol (MeOH) was used as an irreversible electron donor (<0.1 μmol h⁻¹), indicating the inertness of InHCF for H₂ evolution.

Figure 6 shows the photoelectrochemical measurement results for InHCF/TaON and unmodified TaON particles deposited on a conductive FTO electrode. InHCF modification led to a 7- to 12-fold increase in the photocurrent in the presence of Fe²⁺, indicating the favorable catalytic activity of the InHCF species for the oxidation of Fe²⁺. As mentioned above, the redox potential of Fe^{III}/Fe^{II} in InHCF was determined to be ≈0.93 V versus SHE at pH = 2.5 (Figure 2c); the photogenerated holes in TaON (valence band maximum of 2.05 V at pH 2.5, estimated based on a previous report^[51]) can thermodynamically oxidize the Fe^{II} species in InHCF. Indeed, an absorption peak at 2190 cm⁻¹, assignable to the C≡N stretching vibration mode of the oxidized form of InHCF, was observed from the ATR-FTIR spectrum of InHCF/RCO/TaON after irradiation for 25 h in the absence of Fe²⁺ (Figure S13f, Supporting Information). In addition, the oxidized forms of InHCF, In[Fe^{III}(CN)₆] (InHCF-ox) particles, were found to oxidize Fe²⁺ cations in aqueous solution at pH 2.5. As shown in Figure S14, Supporting Information, the amount of Fe²⁺ in the solution spontaneously decreased by 15 μmol, accompanied by an increase in Fe³⁺ (11 μmol). Thus, Fe²⁺ oxidation is most likely promoted through the Fe^{III}/Fe^{II} redox cycles in InHCF, whereby the photogenerated holes in TaON oxidize Fe^{II} in InHCF to Fe^{III}, and the resulting Fe^{III} species oxidize Fe²⁺ cations in the solution to Fe³⁺, as illustrated in Scheme 1. It should be noted that InHCF loading on TaON led to an increase in the photocurrent, even in the absence of Fe²⁺ (Figure 6c), suggesting that the InHCF species capture the photogenerated holes in TaON to some extent. Therefore, it

can be concluded that the InHCF nanoparticles loaded onto the TaON photocatalyst surface functioned as an effective facilitator for Fe²⁺ oxidation by the photogenerated holes of TaON, thereby drastically enhancing the H₂ evolution initiated by photoexcited electrons on H₂ evolution cocatalysts, such as RCO.

An important finding was that the combination of InHCF with RCO specifically and drastically promoted H₂ evolution from aqueous Fe²⁺, whereas that of InHCF and conventional Pt did not (Figure 4 and 5). Because metallic Pt exhibits the lowest overpotential for water (or H⁺) reduction,^[52] the loading of Pt as a cocatalyst has been proven to enhance H₂ production by various photocatalysts, including TaON, in the presence of appropriate sacrificial electron donors.^[19,53,54] However, when a reversible redox species, such as Fe²⁺ or I⁻, is used as an electron donor, Pt metal also catalyzes backward reactions, such as the reduction of Fe³⁺ or I₃⁻ (IO₃⁻),^[14,55] significantly lowering the H₂ evolution rate. Indeed, H₂ evolution on Pt/TaON from an aqueous MeOH solution was nearly completely suppressed by the addition of Fe³⁺ cations to the solution (Figure S15, Supporting Information), indicating a preference for Fe³⁺ reduction over that of H⁺. Preferential Fe³⁺ reduction by Pt is further supported by the electrochemical measurement results shown in Figure S16a,b, Supporting Information; Pt (or Rh) loading onto an FTO substrate led to a significant shift in the onset potential of Fe³⁺ reduction from ≈0.4 to ≈0.8 V (vs. SHE). Although a reduction peak was also generated at ≈0.7 V by the RCO-loaded FTO electrode during the cathodic scan (Figure S16c, Supporting Information), it was independent of the Fe³⁺ concentration. In contrast, the reduction peak of RCO with the onset potential of ≈0.4 V increased with increasing Fe³⁺ concentration; the current density of this peak was lower compared to those of Pt and Rh at around 0.8 V. These results indicate that RCO is considerably less active than Pt toward Fe³⁺ reduction, whereas the RCO cocatalyst has been proven to promote H₂ production on various photocatalysts.^[56–58]

The proposed mechanism for the activation of TaON by the coloaded InHCF and RCO cocatalysts is illustrated in Scheme 1 and 2. As with most photocatalysts, the surface of TaON is inactive toward the oxidation of Fe²⁺ cations; therefore,

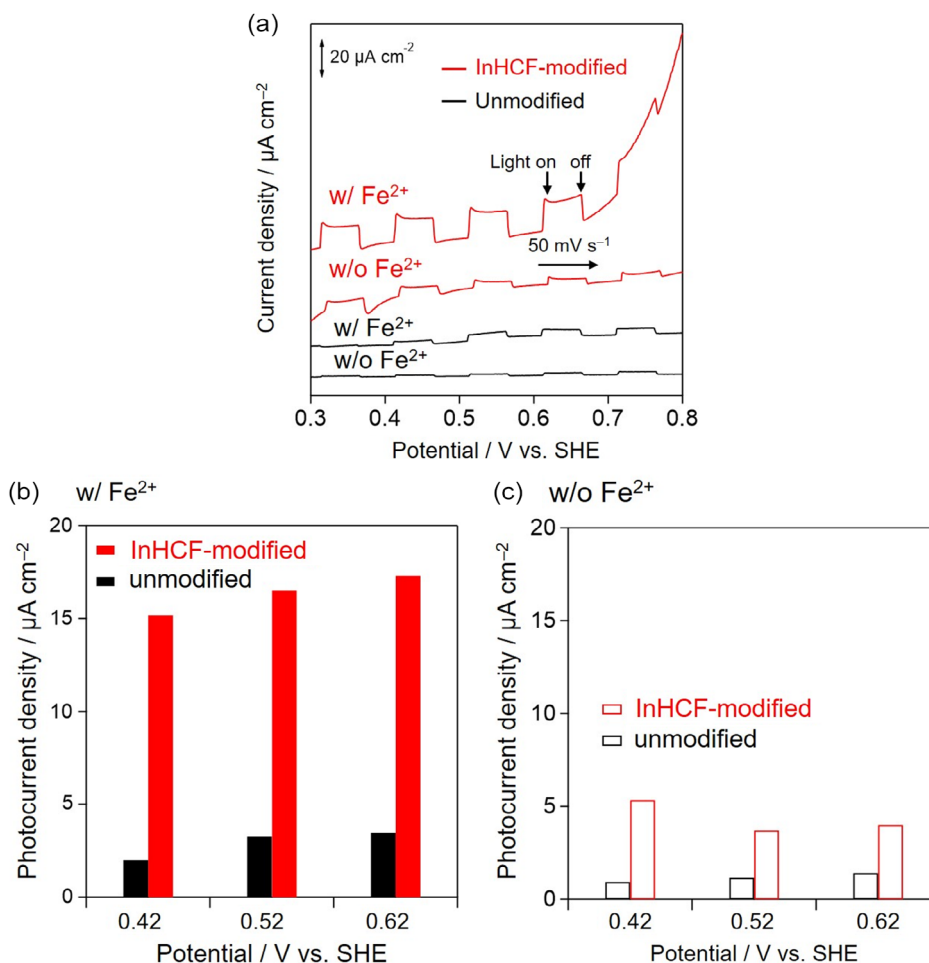


Figure 6. a) I - V curves under chopped visible light irradiation and b,c) photocurrent densities of InHCF-modified or unmodified TaON/FTO in aqueous K_2SO_4 solution (0.1 M, 80 mL) at pH 2.5 b) with (w/) and c) without (w/o) FeCl_2 (1 mM) under visible light irradiation.

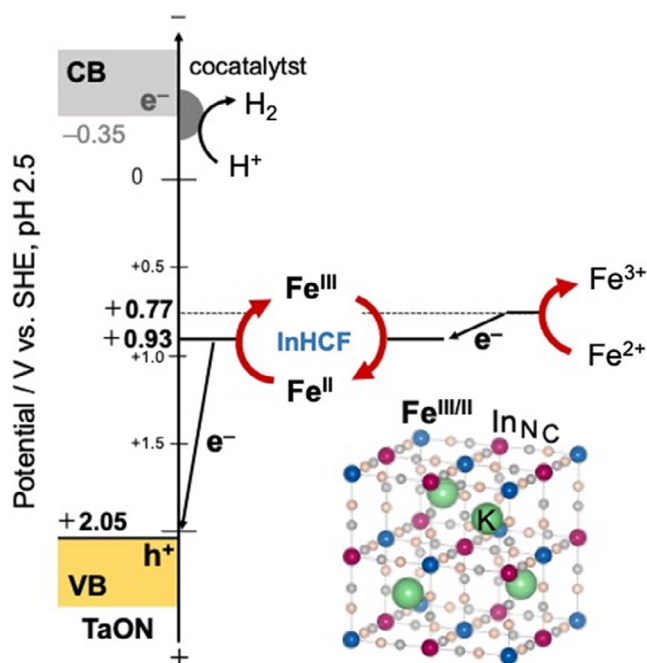
the majority of the photoexcited electrons and photogenerated holes recombine even when the photocatalyst is loaded with an effective H_2 evolution cocatalyst, such as Pt or RCO, resulting in negligible H_2 evolution activity (Scheme 2a). Although InHCF loading can promote the photocatalytic oxidation of Fe^{2+} cations to Fe^{3+} , the generated Fe^{3+} cations are preferentially reduced back to Fe^{2+} by the coloaded Pt (Scheme 2b). Using RCO as a cocatalyst, which is less active for Fe^{3+} reduction than Pt, water (H^+) reduction by photoexcited electrons and Fe^{2+} oxidation by photogenerated holes proceed efficiently on RCO and InHCF, respectively, ultimately activating the TaON photocatalyst for H_2 production using an Fe^{2+} electron donor (Scheme 2c).

Interestingly, the developed InHCF/RCO/TaON photocatalyst is capable of stoichiometric H_2 evolution (see Figure 4); in other words, it oxidizes Fe^{2+} , even when this cation is present at low concentrations. While the ζ potential of unmodified TaON was considerably positive (+36 mV) at pH 2.5, InHCF modification led to a drastic change in the surface potential to negative values (-14 mV), undoubtedly due to the highly negative values (-51 mV) of InHCF particles. Thus, it appears that InHCF loading facilitates the approach of Fe^{2+} to the InHCF surface, accelerating its oxidation, even at low Fe^{2+} concentrations.

This assumption is supported by the observation of enhanced H_2 evolution in the presence of low concentrations of Fe^{2+} (Figure S17, Supporting Information). On the other hand, the enhanced adsorption of Fe^{3+} seems to be detrimental for H_2 evolution because the undesirable backward reaction (i.e., rereduction of Fe^{3+}) might be proceeded. A series of experiments, however, strongly suggested that the present RCO cocatalyst captures the photoexcited electrons and selectively reduces water to H_2 . This favorable function of RCO cocatalyst probably enables the InHCF loaded on TaON to preferentially react with photogenerated holes, rather than photoexcited electrons, making the Fe^{III} species in InHCF dominant rather than Fe^{II} species during the reaction. Consequently, the adsorption of Fe^{3+} on InHCF particles should not be a significant problem.

2.5. Effects of Various Metal Species in MHCFs on H_2 Evolution and Applicability of Coloaded to other Semiconductor Photocatalysts

ZnHCF and FeHCF, in which either Zn^{II} or Fe^{II} is coordinated by the N atom of the CN ligand, were also deposited on the RCO/



Scheme 1. Proposed mechanism of promoted Fe^{2+} oxidation via $\text{Fe}^{\text{III}}/\text{Fe}^{\text{II}}$ redox cycles in InHCF.

TaON photocatalyst. The use of these materials in electrodes for secondary-ion batteries has been well studied.^[59–62] The half-wave potential of $\text{Fe}^{\text{III}}/\text{Fe}^{\text{II}}$ in ZnHCF was determined to be 0.99 V based on its CV profile, while FeHCF provided values of 0.40 V ($\text{Fe}^{\text{III/II}}$ coordinated to N) and 1.07 V ($\text{Fe}^{\text{III/II}}$ coordinated to C) (vs. SHE at pH 2.5). As shown in Figure S18, Supporting Information, these MHCFs also promoted H_2 evolution, although the use of InHCF resulted in the highest rate. While the relationship between the redox potential and the H_2 evolution rate is unclear at present, optimization of the metal species in MHCFs to match the band level of the photocatalyst and the redox potential of the mediator would likely further enhance the oxidation of redox species by photogenerated holes.

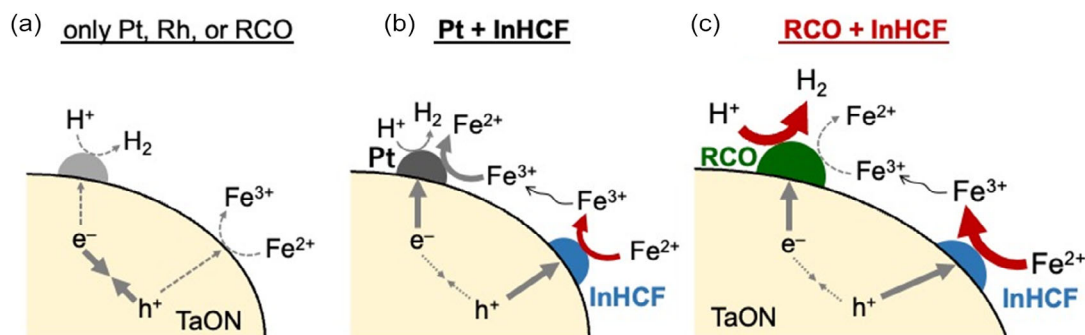
To confirm the utility of the comodification methodology, various photocatalysts that can absorb a wider range of visible light (i.e., Ta_3N_5 (≈ 600 nm),^[63] $\text{Sm}_2\text{Ti}_2\text{S}_2\text{O}_5$ (≈ 650 nm),^[64] and

BaTaO_2N (≈ 650 nm)^[65]) were modified with InHCF after loading them with an RCO reduction cocatalyst. As shown in Figure S19 and Table S1, Supporting Information, the H_2 evolution activities markedly improved in all cases, indicating the versatility of this method for amplifying H_2 evolution in the presence of Fe^{2+} electron donors. Note that the loading amounts of InHCF and RCO were not optimized; hence, further improvements in the activity are possible. Moreover, the synthesis of photocatalyst particles can be optimized to maximize their desired properties. Recently, the development of synthetic procedures for accessing various photocatalyst materials with superior properties has been intensively studied.^[66,67] Considering these factors, further enhancements can be expected for the proposed system.

2.6. Z-Scheme Water Splitting with $\text{Fe}^{3+}/\text{Fe}^{2+}$ Redox Couple Using InHCF/RCO/TaON as H_2 Evolution Photocatalyst

InHCF/RCO/TaON was employed as HEP in Zs-WS with an $\text{Fe}^{3+}/\text{Fe}^{2+}$ redox mediator in combination with BiVO_4 ,^[68] which has been extensively employed as OEP in $\text{Fe}^{3+}/\text{Fe}^{2+}$ mediated Zs-WS. As shown in Figure 7, this combination afforded simultaneous evolution of H_2 and O_2 under visible light. The amount of evolved H_2 was more than twice that of O_2 in the initial stages of illumination because the reactions were initiated by the presence of Fe^{2+} only. After the evacuation of the gas phase, the rates of H_2 and O_2 evolution eventually approached a near-stoichiometric ratio (2:1); the amount of H_2 and O_2 evolved from 10 to 35 h (i.e., during second run) was 497 and 243 μmol , respectively. The total amount of H_2 produced after 35 h of operation (887 μmol) was greater than the amount of Fe^{2+} present (500 μmol). The turnover number of the reacted electrons per mole of Fe^{2+} was calculated to be 3.5, indicating that the overall water splitting proceeds via the $\text{Fe}^{3+}/\text{Fe}^{2+}$ redox relay. Note that the gas evolution was negligible when the RCO/TaON sample without InHCF was employed (open squares), confirming that modification with InHCF as a cocatalyst for Fe^{2+} oxidation is essential for achieving Zs-WS. This combination of photocatalysts exhibits negligibly low activity in the absence of $\text{Fe}^{3+}/\text{Fe}^{2+}$ at pH 2.5 (open triangles).

As for the combination with the Cs-treated WO_3 (Cs- WO_3) (Figure 8), a simultaneous generation of H_2 and O_2 was also confirmed. Water splitting using the combination InHCF/RCO/



Scheme 2. Proposed mechanism for H_2 evolution using Fe^{2+} electron donor on TaON modified with a) only H_2 evolution cocatalyst, b) Pt and InHCF, and c) RCO and InHCF.

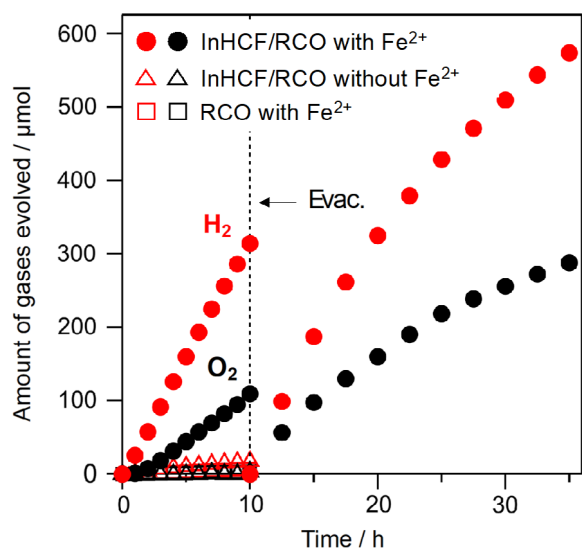


Figure 7. Time courses of gas evolution under visible light irradiation in combination of InHCF/RCO/TaON and BiVO₄ in the presence of 2 mM of FeCl₂ (filled circles) and the absence of FeCl₂ (open triangles) in aqueous solution (250 mL, pH 2.5), along with those in combination of RCO/TaON and BiVO₄ in the presence of FeCl₂ (open squares).

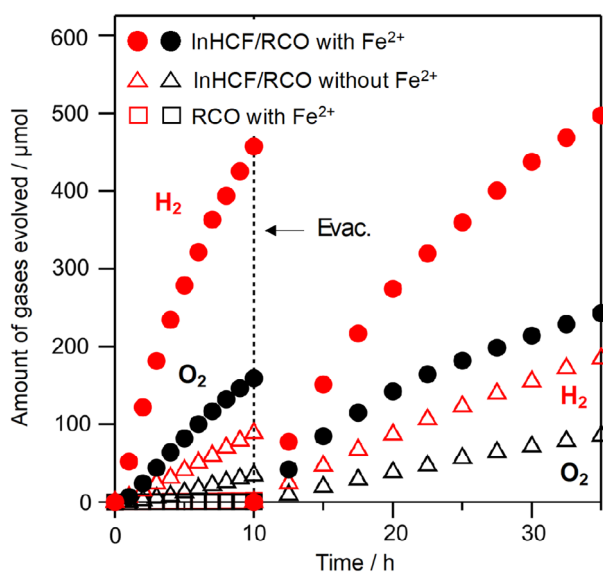


Figure 8. Time courses of gas evolution under visible light irradiation in combination of InHCF/RCO/TaON and Cs-WO₃ in the presence of 2 mM of FeCl₂ (filled circles) and the absence of FeCl₂ (open triangles) in aqueous solution (250 mL, pH 2.5), along with those in combination of RCO/TaON and Cs-WO₃ in the presence of FeCl₂ (open squares).

TaON and Cs-WO₃ with Fe³⁺/Fe²⁺ also proceeded under simulated sunlight irradiation (AM1.5 G) (see Figure S20, Supporting Information), with an STH conversion efficiency of 0.05%. This value is comparable to that of the combination of SrTiO₃:Rh, BiVO₄, and Fe³⁺/Fe²⁺ (0.07–0.1%).^[69,70] In analogy with the BiVO₄ system, the absence of InHCF resulted in negligibly low rates of gas evolution, indicating the necessity of

InHCF as the facilitator for Fe²⁺ oxidation. In stark contrast to the BiVO₄ case, simultaneous evolution of H₂ and O₂ also proceeded even in the absence of Fe³⁺/Fe²⁺, while the rates were lower compared to the case with Fe³⁺/Fe²⁺ redox in the solution. This finding strongly suggested the progress of “interparticle” Zs-WS in this photocatalyst combination. The validity will be discussed in the next section.

2.7. Interparticle Z-Scheme Water Splitting Using InHCF/RCO/TaON as H₂ Evolution Photocatalyst

To testify the progress of interparticle Zs-WS in the combination of InHCF/RCO/TaON and Cs-WO₃ photocatalysts, reactions were carried out under various conditions. One of the possible reasons for the steady and simultaneous H₂ and O₂ evolution even in the absence of Fe³⁺/Fe²⁺ redox added (Figure 8) is the contribution of Fe cation species dissolved from Cs-WO₃ (see Experimental Section) and/or InHCF particles. **Figure 9** shows the results on reactions in pure water wherein the pH of solution spontaneously changed to be about 4.4 after addition of InHCF/RCO/TaON and Cs-WO₃ undoubtedly due to the acidic nature of WO₃ surface. Visible light irradiation to this combination afforded simultaneous and steady evolution of H₂ and O₂ with nearly stoichiometric ratio (closed circles). It is well known that Fe³⁺/Fe²⁺ redox cycle in aqueous solution can't be continued due to the precipitation of Fe³⁺ species as Fe(OH)₃ at pH higher than 3. Indeed as shown in Figure S21, Supporting Information, the same combination in an aqueous FeCl₂ solution at pH 4.4 (adjusted by KOH) resulted in obvious decrease in gas evolution rates with much smaller amount of O₂ gas than the stoichiometric ratio most likely due to the precipitation of Fe(OH)₃ during the reaction. These findings eliminate the possibility that the dissolved Fe cations functioned

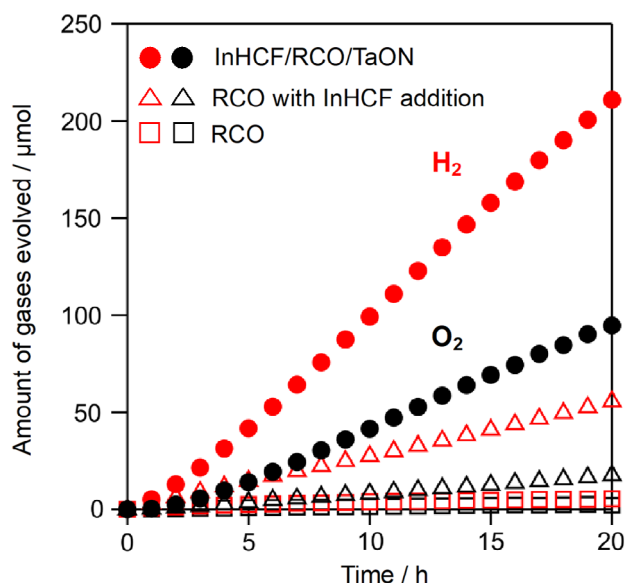
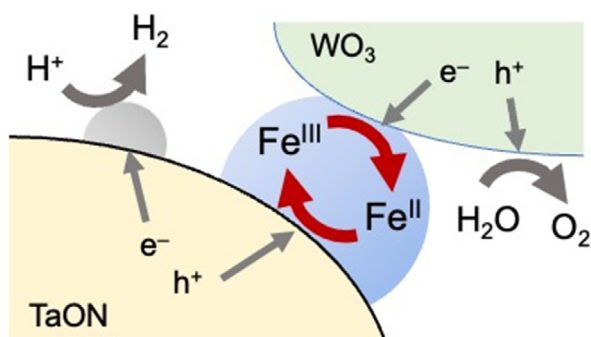


Figure 9. Time courses of gas evolution under visible light irradiation on combination of InHCF/RCO/TaON and Cs-WO₃ in aqueous solution (250 mL, pH 4.4), along with those on combination of RCO/TaON and Cs-WO₃ in the presence or absence of InHCF particles added to solution.



Scheme 3. Proposed mechanism for interparticle Z-scheme water splitting via InHCF solid electron mediator.

as the redox mediator for Zs-WS under this condition (pH 4.4). As shown in Figure 9, gas evolution was negligible in the absence of InHCF loading (open squares), while the simple addition of InHCF particles resulted in lower but appreciable rates of H₂ and O₂ (open triangles), indicating the indispensability of InHCF. Thus, other possible species contributing to Zs-WS will be In³⁺ and [Fe(CN)₆]⁴⁻, dissolved from InHCF. However, the addition of either of them to the reaction solution failed to split water, as shown in Figure S22, Supporting Information, where only small amounts of gasses evolved.

Based on these results, we can now conclude that the InHCF nanoparticles function as solid electron mediators for achieving interparticle Zs-WS via Fe^{III}/Fe^{II} redox cycles in InHCF, as illustrated in Scheme 3. Although the reason for negligible activity of BiVO₄ in the present interparticle Zs-WS is unclear at present, more systematic experiments including pH control will be carried out to clarify the detailed reaction mechanism and thereby improve the efficiency of interparticle Zs-WS utilizing MHCs as facilitators.

3. Conclusion

In summary, we successfully activated TaON to deliver an efficient HEP for both Fe³⁺/Fe²⁺ redox-mediated and interparticle Zs-WS systems. Although TaON has so far been inactive for H₂ evolution in both systems, most likely due to the lack of appropriate oxidation sites, simple surface modification with indium hexacyanoferrate (InHCF) and Rh–Cr mixed oxide (RCO) enabled the efficient production of H₂ by the TaON photocatalyst. The vital roles of InHCF determined to entail the promotion of Fe²⁺ oxidation or interparticle electron transfer via Fe^{III}/Fe^{II} redox cycles in the structure.

The present study achieved two important advancements. First is the enhanced oxidation of the redox mediator, shown to be instrumental in achieving efficient Zs-WS, which has not been examined systematically to date.^[41,42,64] This strategy indeed overcomes the long-standing limitation in Zs-WS with Fe³⁺/Fe²⁺, that is, the rhodium-doped SrTiO₃ has been the most favorable choice as an efficient HEP. The elucidation and harnessing of such oxidation processes will widen the selection of HEPs with narrow bandgaps, such as Ta₃N₅, Sm₂Ti₂S₂O₅, and BaTaO₂N, thereby contributing to the development of highly

efficient Zs-WS systems with various redox mediators. The second is the utilization of MHCs as solid electron mediators for interparticle Zs-WS. The highly diverse family of coordination polymers allows for the precise control of their physicochemical properties to customize them for targeted reactions, both for various redox-mediated and for interparticle Zs-WS systems. As demonstrated in various research fields,^[35,36,39,40,42,71–73] critical MHC properties, such as catalytic activity and redox potential, can be modified by varying the metal cation or ligand, enabling the development of more effective cocatalysts capable of enhancing each reaction involved in Zs-WS.

4. Experimental Section

Sample Preparation: ZrO₂-modified TaON particles as the model HEP were synthesized by a previously reported method with a modification.^[53,74] First, ZrO(NO₃)₂·2H₂O (99.0%; Kanto Chemical Co., Inc.) and Ta₂O₅ (99.9%; Kojundo Chemical Laboratory Co., Ltd.) powders were mixed with a small amount of methanol (MeOH, 99.8%; FUJIFILM Wako Pure Chemical Corporation). The molar ratio of Zr to Ta was set to be 0.1. After being dried in an oven at 343 K for 1 h, the resulting powder was heated in air at 1073 K for 2 h using an Al₂O₃ crucible. Then, the as-prepared ZrO₂/Ta₂O₅ powder was calcined at 1123 K for 15 h under NH₃ flow (12 mL min⁻¹). As-prepared ZrO₂-modified TaON particles were confirmed to be similar to the previously-reported one^[74] (Figure S23, Supporting Information). ZrO₂-modified TaON was denoted as TaON for simplicity.

BaTaO₂N,^[65,66] Ta₃N_{5,^[63] and Sm₂Ti₂S₂O_{5^[64] were synthesized as another HEP, according to the literature. BiVO_{4^[68] and Cs-treated WO_{3^[75,76] as O₂ evolution photocatalysts (OEPs) for Z-scheme water splitting were prepared according to the previous reports. As for the surface treatment of WO₃ particles, CsCl and FeSO₄·7H₂O were used in the modification process according to the previous reports.}}}}

Indium hexacyanoferrate (denoted as InHCF, composition: KIn[Fe(CN)₆]) nanoparticles were prepared by a coprecipitation method by referencing the previous report.^[44] An aqueous solution 30 mL of InCl₃·4H₂O (30 mmol, 99.95%; Kanto Chemical Co., Inc.) was added to an aqueous solution 60 mL of K₄[Fe(CN)₆]·3H₂O (30 mmol, 99.5%; Kishida Chemical Co., Ltd.). The reaction mixture was vigorously stirred for 5 min using a magnetic stirrer. The resulting precipitate was centrifuged (3700 rpm), washed with water three times and MeOH once, and dried in an oven at 308 K under vacuum. InHCF particles were characterized by a series of experiments (Figure 2, S1, and S2, Supporting Information).

The oxidized form of InHCF (denoted as InHCF-ox) was also synthesized by the above method, except for the use of K₃[Fe(CN)₆] (30 mmol, 99.0%; FUJIFILM Wako Pure Chemical Corporation) instead of K₄[Fe(CN)₆]·3H₂O. Zinc hexacyanoferrate (K₂Zn₃[Fe(CN)₆]₂, ZnHCF) and iron(II) hexacyanoferrate (K₂Fe^{II}[Fe(CN)₆], FeHCF) were also synthesized by the above method for InHCF preparation, except for the use of ZnBr₂ (45 mmol, 99.9%; FUJIFILM Wako Pure Chemical Corporation) and FeCl₂·4H₂O (30 mmol, 99.0%; FUJIFILM Wako Pure Chemical Corporation), respectively, instead of InCl₃·4H₂O.

Surface Modification: Any one of Pt, Rh, or Rh_xCr_{2-x}O₃ species as H₂ evolution cocatalysts was loaded on TaON particles, as follows. Pt particles were loaded onto TaON by an impregnation method. TaON powder was immersed in an aqueous solution containing the required amount of H₂PtCl₆·6H₂O (99.9%; FUJIFILM Wako Pure Chemical Corporation) and placed into a hot water bath. After the solution was evaporated, the resulting powder was calcined at 473 K for 1 h under H₂ flow (20 mL min⁻¹). Rh and Rh_xCr_{2-x}O_{3^[56]} particles were loaded on TaON by a photodeposition method. TaON powder was immersed in an aqueous MeOH solution (20 vol%) containing the required amount of Na₃RhCl₆·nH₂O (>80.0%; Kanto Chemical Co., Inc.) or both Na₃RhCl₆·nH₂O and K₂CrO₄ (99.0%; FUJIFILM Wako Pure Chemical Corporation) for Rh and Rh_xCr_{2-x}O₃,

respectively. The suspension was purged by Ar gas to remove dissolved air and then exposed to visible light ($\lambda > 400$ nm) through a 300 W Xe lamp (LX-300F, Cermax) equipped with a CM-1 cold mirror and a cutoff filter (HOYA, L42) under Ar bubbling (50 mL min^{-1}). The Rh- or $\text{Rh}_x\text{Cr}_{2-x}\text{O}_3$ -deposited samples were collected by filtration and then dried in an oven at 308 K under vacuum. Each deposited reduction cocatalyst was determined by XPS and X-ray absorption fine structure (XAFS) spectroscopy (Figure S24 and S25, Supporting Information). Unless otherwise noted, the amount of added Pt or Rh precursor was set to be 1 wt% as each metal with respect to TaON and that of added Cr was set to 1.5 wt%, based on the results in Table 1.

Reduction-cocatalysts-loaded or unloaded TaON powder was modified with InHCF nanoparticles through an impregnation method. TaON samples were immersed in a water dispersed with a certain amount of InHCF particles. The solution was dried up and then heated at 373 K for 1 h under Ar flow (20 mL min^{-1}). Unless otherwise noted, the loading amount of InHCF was 10 mol% as Fe in InHCF with respect to TaON based on the results in Table 1. Note that the loading amount was calculated assuming that the formula of InHCF nanoparticles was $\text{KIn}[\text{Fe}(\text{CN})_6]$. InHCF-modified sample was denoted as $\text{InHCF}/\text{Rh}_x\text{Cr}_{2-x}\text{O}_3/\text{TaON}$, for example. For a control experiment, the modification with InCl_3 instead of InHCF nanoparticles was conducted via the same procedure.

Characterization: The prepared samples were characterized by powder XRD (Mini Flex II, Rigaku, X-ray source; Cu K α) measurement, ICP-optical emission spectroscopy (ICP-OES; iCAP 7400 ICP-OES Duo, Thermo Fisher Scientific Inc.), UV-visible diffuse reflectance spectroscopy (UV-vis DRS; V-650, JASCO), and ATR-FTIR (ATR; ATR Pro One, JASCO, FT-IR; FT-4200, JASCO) using a diamond prism. ATR-FTIR spectra were recorded against air as a background. The crystal structures were drawn using the VESTA program.^[77] The samples were also characterized by scanning electron microscopy (SEM; NVision 40, Carl Zeiss-SIINT), TEM (JEM-2100F, JEOL), and XPS (MT-5500, ULVAC-PHI, Inc., X-ray source: Mg K α). The binding energies in XPS were calibrated with reference to the Au 4f_{7/2} peak position (84.0 eV) of the deposited Au metal on the samples. XAFS experiments were carried out at the PF-AR NW10A. The BET surface area was measured by using a BELSORP-mini II (Microtrac BEL) at liquid nitrogen temperature (77 K). ζ potentials of InHCF/TaON, TaON and InHCF were measured in aqueous solution using a ζ potential analyzer (Zetasizer Nano ZS, Malvern Instruments). The pH of the solution was adjusted by aqueous HCl or KOH.

Electrochemical and Photoelectrochemical Measurements: InHCF, TaON, and InHCF/TaON electrodes were prepared on a FTO glass by a squeegee method. A slurry of the respective samples in water was pasted on a FTO glass and then heated at 373 K for 1 h under Ar flow (20 mL min^{-1}). The coated area and the deposited amount were fixed at approximately $1.5 \times 1.5 \text{ cm}^2$ and $1.0 \pm 0.3 \text{ mg}$, respectively.

The reduction cocatalyst (i.e., Pt, Rh or $\text{Rh}_x\text{Cr}_{2-x}\text{O}_3$)-deposited electrode was prepared through a spin-coating technique. For the deposition of Pt or Rh species, a methanol-water mixed solution (1:1, 20 μL) containing $\text{H}_2\text{PtCl}_6 \cdot 6\text{H}_2\text{O}$ or $\text{Rh}(\text{NO}_3)_3$ (10 mM, 80.0%; Kanto Chemical Co., Inc.) was dropped on a conductive fluorine-doped tin oxide (FTO) glass ($1.5 \times 2.5 \text{ cm}^2$), spin coated (500 rpm, 5 s followed by 1000 rpm, 120 s), and then heated at 473 K for 1 h under an H_2 flow (20 mL min^{-1}). For $\text{Rh}_x\text{Cr}_{2-x}\text{O}_3$, the same procedure was applied except for the use of a methanol-water mixed solution (1:1, 20 μL) containing $\text{Rh}(\text{NO}_3)_3$ (10 mM) and $\text{Cr}(\text{NO}_3)_3$ (30 mM, 98.0–103.0%; Kanto Chemical Co., Inc.) and calcination at 673 K in air.

Electrochemical or photoelectrochemical measurements were performed in an aqueous solution of K_2SO_4 (0.1 M, 99.0%; FUJIFILM Wako Pure Chemical Corporation, pH 2.5, adjusted by H_2SO_4) as an electrolyte under Ar atmosphere using a three-electrode cell. The prepared electrode as the working electrode, Pt coil as the counter electrode, Ag/AgCl as the reference electrode were connected to a potentiostat (VersaSTAT 4, AMETEK), and then cyclic voltammograms or linear sweep voltammograms were recorded. For photoelectrochemical measurement, the photocatalyst electrodes were irradiated with intermittent visible light ($\lambda > 400$ nm) by a 300 W Xe lamp equipped with a CM-1 cold mirror and an L-42 cutoff filter. In some cases, $\text{FeCl}_3 \cdot 6\text{H}_2\text{O}$ (5–20 mM, 99.0%–

102.0%; FUJIFILM Wako Pure Chemical Corporation) or $\text{FeCl}_2 \cdot 4\text{H}_2\text{O}$ (1 mM) was added to the electrolyte solution.

Photocatalytic Reactions: Photocatalytic reactions were conducted in Pyrex side-illuminated reaction vessel connected to a glass closed gas-circulation system. A 300 W Xe lamp was used as a light source in combination with a CM-1 cold mirror and an L-42 cutoff filter for illumination with visible light ($\lambda > 400$ nm). For the photocatalytic H_2 evolution, the prepared photocatalyst powder (0.05 g) was dispersed in 250 mL of aqueous FeCl_2 solution (5 mM, pH 2.5 adjusted with HCl to prevent the deposition of $\text{Fe}(\text{OH})_3$). The suspension was irradiated with visible light after thoroughly degassed and purged with Ar. The evolved gases were analyzed by a gas chromatography unit (GC-8A, Shimadzu, TCD detector, MS 5A column, Ar carrier) directly connected to the closed gas-circulation system. In some cases, aqueous FeCl_2 solution (1 or 2.5 mM, pH 2.5) or aqueous MeOH solution (20 vol%) was used as the reaction solution. To measure the apparent quantum efficiency (AQE), a monochromatic light ($\lambda = 420$ nm) was used with a Xe lamp (MAX-303, Asahi Spectra Co., Ltd.).

For the photocatalytic Z-scheme water splitting under visible light, the same experimental setting was applied, except the use of BiVO_4 or the Cs-treated WO_3 powder in addition to the $\text{InHCF}/\text{Rh}_x\text{Cr}_{2-x}\text{O}_3/\text{TaON}$ photocatalyst (0.05 g each) and an aqueous FeCl_2 solution (2 mM, pH 2.5 adjusted with HCl). For the interparticle Z-scheme reactions, the photocatalysts were suspended in pure water (i.e., in the absence of FeCl_2), while in some cases HCl or KOH was added to adjust pH value. Z-scheme water splitting was also conducted under the simulated solar irradiation. A solar simulator (HAL-320, ASAHI SPECTRA, AM 1.5G, 100 mW cm^{-2}) was used as a light source. $\text{InHCF}/\text{Rh}_x\text{Cr}_{2-x}\text{O}_3/\text{TaON}$ and the Cs-treated WO_3 powder (0.05 g each) were dispersed in 100 mL of aqueous FeCl_2 solution (2 mM, pH 2.5 adjusted with HCl). After thoroughly degassed and purged with Ar, the suspension was irradiated with the solar simulator. The evolved gases were analyzed by a gas chromatography unit (GC-8A, Shimadzu, TCD detector, MS 5A column, Ar carrier) directly connected to the closed gas-circulation system. STH was determined by Equation (2).

$$\text{STH} (\%) = (R(\text{H}_2) \times \Delta G) / (P \times S) \times 100 \quad (2)$$

where $R(\text{H}_2)$, ΔG , P , and S , respectively describe the rate of H_2 evolution during the water splitting, the Gibbs energy for the reaction (237 kJ mol^{-1}), the photon energy intensity (100 mW cm^{-2}), and the irradiation area ($\approx 15 \text{ cm}^2$).

Chemical Reaction of Fe^{2+} and an Oxidized form of InHCF (InHCF-ox): InHCF-ox (100 μmol as $\text{In}[\text{Fe}^{\text{III}}(\text{CN})_6]$) powder was added to 100 mL of aqueous FeCl_2 solution (0.9 mM, pH 2.5 adjusted by 1 M HCl), and then the solution was stirred by a magnetic stirrer in the dark. The quantitative analysis of Fe^{2+} and Fe^{3+} in the solution was performed by a colorimetric method as follows. A portion of sample aliquots (1 mL) was withdrawn from the solution after each interval of stirring and filtered by a syringe filter (Millex, Millipore) to remove the InHCF-ox particles. As for Fe^{2+} , 50 μL of the supernatant solution was added to the mixture of 2,4,6-tris(2-pyridyl)-1,3,5-triazine (TPTZ; 1.0 mM, 700 μL) and acetate buffer (pH 5.2, 2 M, 2.1 mL) in a quartz cell to form the $\text{Fe}(\text{II})$ -TPTZ complex.^[78,79] The amount of Fe^{2+} was determined based on the peak absorbance at 597 nm attributed to $\text{Fe}(\text{II})$ -TPTZ complex using UV-vis spectroscopy (UV-1800, Shimadzu). As for Fe^{3+} , 500 μL of the filtered solution after the reaction and 2000 μL of HCl (6 M) were mixed in a quartz cell, and then the UV-vis absorption spectra of the solution were measured. The amount of dissolved Fe^{3+} was estimated based on the absorbance at 430 nm.

Supporting Information

Supporting Information is available from the Wiley Online Library or from the author.

Acknowledgements

This work was supported by JSPS KAKENHI (JP20H00398) in Grant-in-Aid for Scientific Research (A), JSPS Research Fellow (grant number 19J23359), and JSPS KAKENHI (JP17H06439, JP17H06438) in Scientific Research on Innovative Area “Innovations for Light-Energy Conversion (I4LEC).” The authors are grateful to Dr. Rie Haruki and Dr. Tomoki Kanazawa of KEK for their helpful support in X-ray absorption fine structure measurement.

Conflict of Interest

The authors declare no conflict of interest.

Data Availability Statement

The data that support the findings of this study are available from the corresponding author upon reasonable request.

Keywords

artificial photosynthesis, photocatalysts, visible light, water splitting, Z-schemes

Received: June 6, 2023
Revised: July 10, 2023
Published online: July 30, 2023

- [1] A. Kudo, Y. Miseki, *Chem. Soc. Rev.* **2009**, *38*, 253.
- [2] R. Abe, *Bull. Chem. Soc. Jpn.* **2011**, *84*, 1000.
- [3] B. A. Pinaud, J. D. Benck, L. C. Seitz, A. J. Forman, Z. Chen, T. G. Deutsch, B. D. James, K. N. Baum, G. N. Baum, S. Ardo, H. Wang, E. Miller, T. F. Jaramillo, *Energy Environ. Sci.* **2013**, *6*, 1983.
- [4] M. R. Shaner, H. A. Atwater, N. S. Lewis, E. W. McFarland, *Energy Environ. Sci.* **2016**, *9*, 2354.
- [5] Q. Wang, K. Domen, *Chem. Rev.* **2020**, *120*, 919.
- [6] K. Maeda, K. Teramura, D. Lu, T. Takata, N. Saito, Y. Inoue, K. Domen, *Nature* **2006**, *440*, 440295.
- [7] K. Maeda, D. Lu, K. Domen, *Chem. Eur. J.* **2013**, *19*, 4986.
- [8] R. Asai, H. Nemoto, Q. Jia, K. Saito, A. Iwase, A. Kudo, *Chem. Commun.* **2014**, *50*, 2543.
- [9] Q. Wang, M. Nakabayashi, T. Hisatomi, S. Sun, S. Akiyama, Z. Wang, Z. Pan, X. Xiao, T. Watanabe, T. Yamada, N. Shibata, T. Takata, K. Domen, *Nat. Mater.* **2019**, *18*, 827.
- [10] F. A. Chowdhury, M. L. Trudeau, H. Guo, Z. Mi, *Nat. Commun.* **2018**, *9*, 1707.
- [11] H. Li, J. Xiao, J. J. M. Vequizo, T. Hisatomi, M. Nakabayashi, Z. Pan, N. Shibata, A. Yamakata, T. Takata, K. Domen, *ACS Catal.* **2022**, *12*, 10179.
- [12] K. Chen, J. Xiao, J. J. M. Vequizo, T. Hisatomi, Y. Ma, M. Nakabayashi, T. Takata, A. Yamakata, N. Shibata, K. Domen, *J. Am. Chem. Soc.* **2023**, *145*, 3839.
- [13] A. Kudo, *MRS Bull.* **2011**, *36*, 32.
- [14] Y. Wang, H. Suzuki, J. Xie, O. Tomita, D. J. Martin, M. Higashi, D. Kong, R. Abe, J. Tang, *Chem. Rev.* **2018**, *118*, 5201.
- [15] R. Abe, K. Sayama, H. Sugihara, *J. Phys. Chem. B* **2005**, *109*, 16052.
- [16] H. Kato, M. Hori, R. Kenta, Y. Shimodaira, A. Kudo, *Chem. Lett.* **2004**, *33*, 1348.
- [17] D. J. Martin, P. J. T. Reardon, S. J. A. Moniz, J. Tang, *J. Am. Chem. Soc.* **2014**, *136*, 12568.
- [18] Y. Bai, K. Nakagawa, A. J. Cowan, C. M. Aitchison, Y. Yamaguchi, M. A. Zwijnenburg, A. Kudo, R. S. Sprick, A. I. Cooper, *J. Mater. Chem. A* **2020**, *8*, 16283.
- [19] R. Kenta, T. Ishii, H. Kato, A. Kudo, *J. Phys. Chem. B* **2004**, *108*, 8992.
- [20] H. Suzuki, O. Tomita, M. Higashi, R. Abe, *Chem. Lett.* **2015**, *44*, 1134.
- [21] H. Suzuki, O. Tomita, M. Higashi, R. Abe, *J. Mater. Chem. A* **2017**, *5*, 10280.
- [22] A. Nakada, S. Nishioka, J. J. M. Vequizo, K. Muraoka, T. Kanazawa, A. Yamakata, S. Nozawa, H. Kumagai, S. Adachi, O. Ishitani, K. Maeda, *J. Mater. Chem. A* **2017**, *5*, 11710.
- [23] H. Fujito, H. Kunioku, D. Kato, H. Suzuki, M. Higashi, H. Kageyama, R. Abe, *J. Am. Chem. Soc.* **2016**, *138*, 2082.
- [24] Y. Sasaki, H. Nemoto, K. Saito, A. Kudo, *J. Phys. Chem. C* **2009**, *113*, 17536.
- [25] A. Iwase, Y. H. Ng, Y. Ishiguro, A. Kudo, R. Amal, *J. Am. Chem. Soc.* **2011**, *133*, 11054.
- [26] Q. Wang, T. Hisatomi, Q. X. Jia, H. Tokudome, M. Zhong, C. Z. Wang, Z. H. Pan, T. Takata, M. Nakabayashi, N. Shibata, Y. B. Li, I. D. Sharp, A. Kudo, T. Yamada, K. Domen, *Nat. Mater.* **2016**, *15*, 611.
- [27] Q. Wang, S. Okunaka, H. Tokudome, T. Hisatomi, M. Nakabayashi, N. Shibata, T. Yamada, K. Domen, *Joule* **2018**, *2*, 2667.
- [28] B.-J. Ng, L. K. Putri, X. Y. Kong, P. Pasbakhsh, S.-P. Chai, *Chem. Eng. J.* **2021**, *404*, 127030.
- [29] A. Iwase, S. Yoshino, T. Takayama, Y. H. Ng, R. Amal, A. Kudo, *J. Am. Chem. Soc.* **2016**, *138*, 10260.
- [30] Y. Sasaki, H. Kato, A. Kudo, *J. Am. Chem. Soc.* **2013**, *135*, 5441.
- [31] N. R. De Tacconi, K. Rajeshwar, R. O. Lezna, *Chem. Mater.* **2003**, *15*, 3046.
- [32] D. M. DeLongchamp, P. T. Hammond, *Adv. Funct. Mater.* **2004**, *14*, 224.
- [33] E. Kholoud, H. Watanabe, A. Takahashi, M. M. Emara, B. A. Abd-El-Nabey, M. Kurihara, K. Tajima, T. Kawamoto, *J. Mater. Chem. C* **2017**, *5*, 8921.
- [34] A. Kitajima, H. Tanaka, N. Minami, K. Yoshino, T. Kawamoto, *Chem. Lett.* **2012**, *41*, 1473.
- [35] A. Takahashi, H. Tanaka, D. Parajuli, T. Nakamura, K. Minami, Y. Sugiyama, Y. Hakuta, S. I. Ohkoshi, T. Kawamoto, *J. Am. Chem. Soc.* **2016**, *138*, 6376.
- [36] Y. Lu, L. Wang, J. Cheng, J. B. Goodenough, *Chem. Commun.* **2012**, *48*, 6544.
- [37] K. Hurlbutt, S. Wheeler, I. Capone, M. Pasta, *Joule* **2018**, *2*, 1950.
- [38] S. Goberna-Ferrón, W. Y. Hernández, B. Rodríguez-García, J. R. Galán-Mascarós, *ACS Catal.* **2014**, *4*, 1637.
- [39] Y. Yamada, K. Oyama, R. Gates, S. Fukuzumi, *Angew. Chem. Int. Ed.* **2015**, *54*, 5613.
- [40] H. Tabe, C. Terashima, Y. Yamada, *Catal. Sci. Technol.* **2018**, *8*, 4747.
- [41] T. Shirakawa, M. Higashi, O. Tomita, R. Abe, *Sustain. Energy Fuels* **2017**, *1*, 1065.
- [42] H. Matsuoka, M. Higashi, A. Nakada, O. Tomita, R. Abe, *Chem. Lett.* **2018**, *47*, 941.
- [43] Y. Kageshima, Y. Gomyo, H. Matsuoka, H. Inuzuka, H. Suzuki, R. Abe, K. Teshima, K. Domen, H. Nishikiori, *ACS Catal.* **2021**, *11*, 8004.
- [44] A. Gotoh, H. Uchida, M. Ishizaki, T. Satoh, S. Kaga, S. Okamoto, M. Ohta, M. Sakamoto, T. Kawamoto, H. Tanaka, M. Tokumoto, S. Hara, H. Shiozaki, M. Yamada, M. Miyake, M. Kurihara, *Nanotechnology* **2007**, *18*, 345609.

- [45] L. Chen, H. Shao, X. Zhou, G. Liu, J. Jiang, Z. Liu, *Nat. Commun.* **2016**, 7, 11982.
- [46] J. Kiener, L. Limousy, M. Jeguirim, J. M. Le Meins, S. Hajjar-Garreau, G. Bigoin, C. M. Ghimbeu, *Materials* **2019**, 12, 1253.
- [47] H. J. Buser, D. Schwarzenbach, W. Petter, A. Ludi, *Inorg. Chem.* **1977**, 16, 2704.
- [48] S. S. Kaye, J. R. Long, *Catal. Today* **2007**, 120, 311.
- [49] P. J. Kulesza, M. Faszynska, *J. Electroanal. Chem.* **1988**, 252, 461.
- [50] Z. Jin, S. Dong, *Electrochim. Acta* **1990**, 35, 1057.
- [51] W. J. Chun, A. Ishikawa, H. Fujisawa, T. Takata, J. N. Kondo, M. Hara, M. Kawai, Y. Matsumoto, K. Domen, *J. Phys. Chem. B* **2003**, 107, 1798.
- [52] S. Trasatti, *J. Electroanal. Chem.* **1972**, 39, 163.
- [53] K. Maeda, M. Higashi, D. Lu, R. Abe, K. Domen, M. Higashi, D. Lu, R. Abe, K. Domen, *J. Am. Chem. Soc.* **2010**, 132, 5858.
- [54] Y. Wang, Y. Wang, R. Xu, *J. Phys. Chem. C* **2013**, 117, 783.
- [55] R. Abe, K. Sayama, H. Arakawa, *J. Photochem. Photobiol., A* **2004**, 166, 115.
- [56] K. Maeda, D. Lu, K. Teramura, K. Domen, *Energy Environ. Sci.* **2010**, 3, 471.
- [57] K. Maeda, K. Teramura, H. Masuda, T. Takata, N. Saito, Y. Inoue, K. Domen, *J. Phys. Chem. B* **2006**, 110, 13107.
- [58] T. H. Chiang, H. Lyu, T. Hisatomi, Y. Goto, T. Takata, M. Katayama, T. Minegishi, K. Domen, *ACS Catal.* **2018**, 8, 2782.
- [59] J. Liao, Q. Hu, Y. Yu, H. Wang, Z. Tang, Z. Wen, C. Chen, *J. Mater. Chem. A* **2017**, 5, 19017.
- [60] D. Cai, X. Yang, B. Qu, T. Wang, *Chem. Commun.* **2017**, 53, 6780.
- [61] H. Lee, Y.-I. Kim, J.-K. Park, J. W. Choi, *Chem. Commun.* **2012**, 48, 8416.
- [62] L. Zhang, L. Chen, X. Zhou, Z. Liu, *Adv. Energy Mater.* **2015**, 5, 1400930.
- [63] G. Hitoki, A. Ishikawa, T. Takata, J. N. Kondo, M. Hara, K. Domen, *Chem. Lett.* **2002**, 31, 736.
- [64] G. Ma, S. Chen, Y. Kuang, S. Akiyama, T. Hisatomi, M. Nakabayashi, N. Shibata, M. Katayama, T. Minegishi, K. Domen, *J. Phys. Chem. Lett.* **2016**, 7, 3892.
- [65] M. Higashi, R. Abe, K. Teramura, T. Takata, B. Ohtani, K. Domen, *Chem. Phys. Lett.* **2008**, 452, 120.
- [66] Z. Wang, Y. Luo, T. Hisatomi, J. J. M. Vequizo, S. Suzuki, S. Chen, M. Nakabayashi, L. Lin, Z. Pan, N. Kariya, A. Yamakata, N. Shibata, T. Takata, K. Teshima, K. Domen, *Nat. Commun.* **2021**, 12, 1005.
- [67] J. Xiao, J. J. M. Vequizo, T. Hisatomi, J. Rabeah, M. Nakabayashi, Z. Wang, Q. Xiao, H. Li, Z. Pan, M. Krause, N. Yin, G. Smith, N. Shibata, A. Brückner, A. Yamakata, T. Takata, K. Domen, *J. Am. Chem. Soc.* **2021**, 143, 10059.
- [68] A. Iwase, H. Kato, A. Kudo, *J. Sol. Energy Eng.* **2010**, 132, 021106.
- [69] H. Kato, Y. Sasaki, N. Shirakura, A. Kudo, *J. Mater. Chem. A* **2013**, 1, 12327.
- [70] H. P. Duong, T. Mashiyama, M. Kobayashi, A. Iwase, A. Kudo, Y. Asakura, S. Yin, M. Kakihana, H. Kato, *Appl. Catal., B* **2019**, 252, 222.
- [71] F. Scholz, A. Dostal, *Angew. Chem., Int. Ed. Engl.* **1995**, 34, 2685.
- [72] M. Aksoy, S. V. K. Nune, F. Karadas, *Inorg. Chem.* **2016**, 55, 4301.
- [73] H. W. Lee, R. Y. Wang, M. Pasta, S. W. Lee, N. Liu, Y. Cui, *Nat. Commun.* **2014**, 5, 5280.
- [74] K. Maeda, H. Terashima, K. Kase, M. Higashi, M. Tabata, K. Domen, *Bull. Chem. Soc. Jpn.* **2008**, 81, 927.
- [75] Y. Miseki, H. Kusama, H. Sugihara, K. Sayama, *J. Phys. Chem. Lett.* **2010**, 1, 1196.
- [76] Y. Miseki, K. Sayama, *Catal. Sci. Technol.* **2019**, 9, 2019.
- [77] K. Momma, F. Izumi, *J. Appl. Crystallogr.* **2011**, 44, 1272.
- [78] G. S. R. Krishnamurti, P. M. Huang, *Talanta* **1990**, 37, 745.
- [79] O. Tomita, S. Nitta, Y. Matsuta, S. Hosokawa, M. Higashi, R. Abe, *Chem. Lett.* **2017**, 46, 221.